DOI 10.5162/Ultrasonic2025/P1.31

Study on a Method for Visualizing Hardened Areas Independent of Vibration Direction in Continuous Shear Wave Elastography

Ren Koda[1], Aoi Kuribara[1], Marie Tabaru[2], and Yoshiki Yamakoshi[1]
[1]Gunma University, 1-5-1, Tenjin-cho, Kiryu-shi, Japan
[2]Institute of Science Tokyo, 4259 Nagatsuta-cho, Midori-ku, Yokohama-shi, Japan
koda@gunma-u.ac.jp

Abstract: We propose two continuous shear wave elastography visualization methods to reveal hardened tissue areas regardless vibration direction. Using a tissue-mimicking phantom, vibrations at 78.1 Hz were applied from both the longitudinal and transverse directions relative to the probe. Small-divided-region shear wave velocity imaging consistently identified stiff inclusions under both conditions, while shear strain imaging clearly highlighted their boundaries. Conventional shear wave velocity imaging, in contrast, showed direction-dependent variability.

Keywords: continuous shear wave elastography, shear wave velocity imaging, shear strain imaging, tissue stiffness, ultrasound imaging

Introduction

Because shear wave velocity (SWV)—the speed at which the shear wave propagates through tissue—depends on the stiffness of the medium, various attempts have been made to evaluate the elasticity of biological tissues using shear waves. One of the earliest theoretical studies in this field was conducted by Oestreicher [1].

Later, a technique was developed in which continuous shear waves at around 50 Hz are generated by a compact actuator integrated with an ultrasound probe, allowing measurement of liver elasticity [2]. Subsequently, a practical method known as Shear Wave Elastography (SWE) was established, utilizing impulsive shear waves generated by acoustic radiation force from a focused ultrasound beam [3, 4]. Although safety limits the amplitude of generated shear waves, SWE enables both wave generation and measurement via the same probe and has been widely adopted clinically.

Yamakoshi et al. proposed the continuous SWE (C-SWE) method to visualize tissue elasticity [5]. By applying low-frequency vibrations from a surface actuator, shear waves appear as periodic Doppler signals in color Doppler mode. This method has been applied to musculoskeletal, liver, and mammary tissues, with elasticity inferred from propagation speed [6, 7, 8]. However, C-SWE traditionally assumes that the wave propagates parallel to the element array of the ultrasound probe, an assumption not always met in breast applications. This study investigates two methods for visualizing the stiffened areas independently of the direction of vibration.

Small divided region SWV estimation

When vibrations with frequencies below approximately 1 kHz are applied using a compact shaker, the vibrations propagate through the target medium as shear waves. Simultaneously, if an ultrasonic pulse is transmitted into the target, the backscattered signal received by the same probe is phase-modulated by the Doppler effect.

The ultrasound signal reflected from position (x, z) can be modeled as:

$$y(x,z) = a \exp\{j(2\pi f_0 t + \Delta\varphi(x,z))\} \quad (1)$$

where $\Delta\varphi(x,z)$ represents the Doppler-induced phase modulation:

$$\Delta\varphi(x,z) = \frac{4\pi f_0}{c}\xi_0 \sin(\omega_b t + \theta(x,z)) \quad (2)$$

with: a: amplitude of the ultrasound, f_0: center frequency of the ultrasound, c: speed of sound, ξ_0: displacement amplitude of the shear wave, ω_b: angular frequency of the shear wave, $\theta(x,z)$: local phase of the shear wave.

To demodulate the received ultrasound signal, quadrature detection is performed using a reference signal defined as:

$$r(t) = exp(j2\pi f_0 t) \quad (3)$$

The output of the quadrature demodulation is:

$$Q(x,z) = y(x,z)r*(t) = aexp(j\Delta\phi(x,z)) \quad (4)$$

Here, * denotes complex conjugation.

DOI 10.5162/Ultrasonic2025/P1.31

The Doppler phase component $\Delta\phi(x,z)$ can thus be extracted by:

$$\Delta\phi(x,z) = \tan^{-1}\left(\frac{\mathrm{Im}(Q(x,z))}{\mathrm{Re}(Q(x,z))}\right) \tag{5}$$

To obtain the complex amplitude, a Fourier analysis of the Doppler signal component is performed at the angular frequency ω_b:

$$F(x,z) = \frac{1}{N\Delta t}\int_0^{N\Delta t} \Delta\phi(x,z) exp(j\omega_b t) dt \tag{6}$$

where:

$$\Delta T = \frac{2\pi}{\omega_b} \tag{7}$$

and N is the number of periods for Fourier analysis. By substituting Eq. (2) into Eq. (6), the complex amplitude $F(x,z)$ becomes:

$$F(x,z) = K\exp(j\theta(x,z)) \tag{8}$$

with

$$K = \frac{2\pi f_0 \xi_0}{c} \tag{9}$$

A small-divided-region (SDR) R within the image domain is considered. This region has a width of Δx in the x-direction and Δz in the z-direction,

Let (x_0, z_0) be the center of the region, where a phase reference point A is set. The complex amplitude in the region is multiplied by the complex conjugate of the value at the reference point:

$$\begin{aligned}\Delta F(x,z) &= F(x,z)F^*(x_0,z_0)\\ &= K^2\exp\left[j(\theta(x,z)-\theta(x_0,z_0))\right]\end{aligned} \tag{10}$$

The phase $\theta_e(x,z)$ of $\Delta F(x,z)$ is:

$$\begin{aligned}\theta_e(x,z) &= \tan^{-1}\left(\frac{\mathrm{Im}(\Delta F(x,z))}{\mathrm{Re}(\Delta F(x,z))}\right)\\ &= \theta(x,z) - \theta(x_0,z_0)\end{aligned} \tag{11}$$

Apply a 2D least squares fitting method to $\theta_e(x,z)$ within the region R, and obtain the first-order coefficients a_x and a_z. These represent the phase gradient and correspond to the wave numbers:

$$k_x = a_x, \quad k_z = a_z \tag{12}$$

The shear wave number k, propagation velocity v, and propagation direction ϕ are then given by:

$$k = \sqrt{k_x^2 + k_z^2}, \quad v = \frac{\omega_b}{k}, \quad \phi = \tan^{-1}\left(\frac{k_z}{k_x}\right) \tag{13}$$

By repeating this process while scanning the region across the entire image domain in both the x and z directions, high-resolution estimation of the shear wave propagation parameters can be achieved.

Shear strain estimation

Consider a three-layer structure in which a relatively soft layer is sandwiched between two stiff layers. When sinusoidal displacements are applied to the upper and lower stiff layers in the x-axis direction, their displacements x_1 and x_2 can be described as:

$$x_1 = a_1\sin(\omega t) \tag{14}$$

$$x_2 = a_2\sin(\omega t + \Delta\theta) \tag{15}$$

The shear strain ε generated within the soft intermediate layer due to the differential motion of the stiff layers is given by:

$$\varepsilon = \frac{\Delta x}{L} = \frac{x_1 - x_2}{L} \tag{16}$$

Substituting Eqs. (14) and (15) into Eq. (16), we obtain:

$$\varepsilon = \frac{b\sin(\omega t + \phi)}{L} \tag{17}$$

where the amplitude b and phase ϕ are given by:

$$b = \sqrt{a_1^2 + a_2^2 - 2a_1a_2\cos\Delta\theta} \tag{18}$$

$$\phi = \begin{cases} \tan^{-1}\left(\dfrac{-a_2\sin\Delta\theta}{a_1 - a_2\cos\Delta\theta}\right) \\ \qquad\qquad \text{if } a_1 - a_2\cos\Delta\theta \geq 0 \\ \tan^{-1}\left(\dfrac{-a_2\sin\Delta\theta}{a_1 - a_2\cos\Delta\theta}\right) + \pi \\ \qquad\qquad \text{if } a_1 - a_2\cos\Delta\theta < 0 \end{cases} \tag{19}$$

Therefore, the magnitude of the shear strain induced in the intermediate layer by shear wave propagation is expressed as:

$$|\varepsilon(t)| = \frac{b}{L} \tag{20}$$

Experiments

Two image reconstructions were performed using a linear array ultrasound probe (Finggal Link, Japan) with 128 active elements and a center frequency of 7.5 MHz. Photographs of the experimental setup used for the phantom are shown in Figure 1(a) and 1(b), with the vibration directions of $\theta = 0°$ and $\theta = 90°$, respectively.

An elastography phantom (ELPT-002; OST, Chiba, Japan) was used. It contains five inclusions of varying elasticities and echogenicities embedded in a background material with lower elasticity. These inclusions simulate the Tsukuba elasticity scores (Table 1). Figure 2 shows a schematic diagram of the phantom.

DOI 10.5162/Ultrasonic2025/P1.31

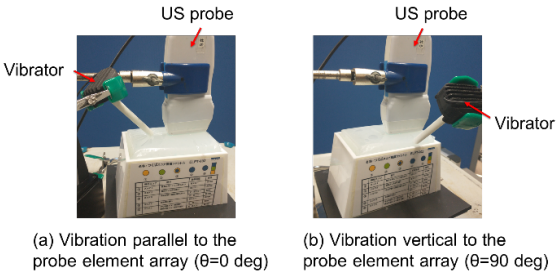

Fig. 1: Vibrator placement for different directions. (a) $\theta = 0°$, (b) $\theta = 90°$

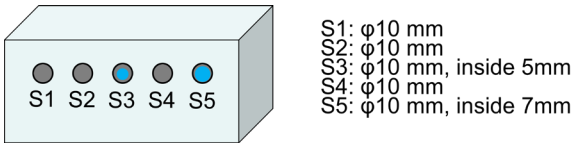

Fig. 2: Schematic image of the tissue-mimicking phantom.

From these, one inclusion corresponding to elasticity score 4 (S4) was selected for imaging. This inclusion has significantly higher stiffness compared to the background.

Results

Figure 3 shows the imaging results of the inclusion with elasticity score 4 under two vibration directions: $\theta = 0°$ (a) and $\theta = 90°$ (b). Images include B-mode, conventional SWV, SDR SWV, and shear strain images in both z and x directions.

The conventional SWV images failed to capture the structural contrast at $\theta = 90°$, whereas SDR SWV maintained visualization consistency across directions. Additionally, shear strain images in both directions exhibited elevated values along inclusion boundaries, regardless of the vibration direction.

Tab. 1: Phantom properties

Score		Brightness	Young's modulus [kPa]
1 (S1)		Low	15
2 (S2)		Low	40
3 (S3)	surroundings	Low	15
	inside	Low	380
4 (S4)		Low	380
5 (S5)	surroundings	stealth	400
	inside	Low	380

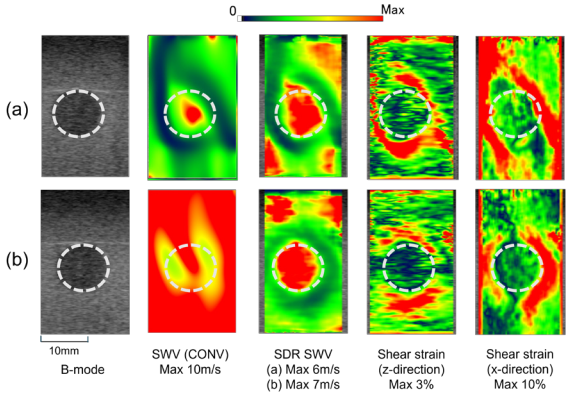

Fig. 3: Imaging results for S4 inclusion under two vibration directions: (a) $\theta = 0°$ and (b) $\theta = 90°$.

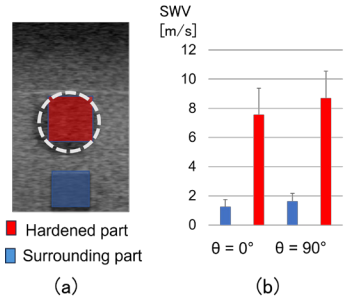

Fig. 4: SDR SWV analysis: (a) ROI setting, (b) Comparison between $\theta = 0°$ and $90°$

Figure 4 shows ROI settings and the SWV values measured within the hardened inclusion and surrounding tissue. The measured velocities were consistent for both vibration directions, closely matching the expected value of 11.22 m/s for the stiff region.

Figure 5 shows results for shear strain. Panel (a) shows the ROI configuration; panels (b) and (c) show z- and x-directional strain respectively. The x-directional strain exhibited overall higher values. There was a consistent and significant contrast between the hardened inclusion and the surroundings in both vibration directions .

Discussion

In this study, it was demonstrated that the two proposed methods enable structural visualization that is independent of the vibration direction. The small-divided-region (SDR) shear wave velocity (SWV) estimation method successfully visualized internal features and similarly, the shear strain method clearly visualized boundary regions, regardless of the vibration direction.

Notably, the shear strain method highlighted large phase differences at the boundary of hardened regions,

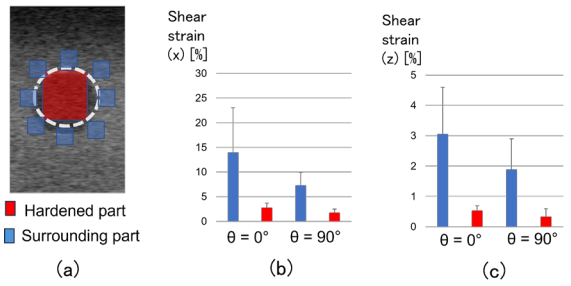

Fig. 5: Shear strain analysis: (a) ROI setting, (b) x-directional shear strain, (c) z-directional shear strain

indicating high shear strain. However, the boundary visualization was not always perfectly aligned, likely due to shear wave refraction effects.

Refraction is influenced by the relationship between excitation direction and target geometry. When there is a large SWV difference between the inclusion and the surrounding medium, the refraction effect becomes more pronounced, resulting in increased variability.

For breast tissue, SWVs for normal breast and malignant lesions have been reported to range from approximately 2.7 to 5.0 m/s. The elastic modulus of normal breast cancer tissue is approximately 22 kPa ([9]), whereas lesions at risk of malignant transformation can reach 74 kPa ([10]). In contrast, the experimental phantom used in this study had a larger SWV contrast, making the results more sensitive to refraction.

Despite improved visualization, the limitations of strain imaging due to unclear tumor boundaries and high variance remain. Future studies will apply directional filters to suppress refractive effects and incorporate simulations and clinical environments to validate and optimize the approach.

Conclusion

In this study, we investigated two methods for visualizing hardened tissue regions independent of vibration direction in continuous shear wave elastography (C-SWE). In phantom experiments, small-divided-region (SDR) SWV estimation visualized internal inclusions consistently, while shear strain imaging highlighted the boundaries of stiff regions. These results demonstrate that both methods can reduce the directional dependency inherent in conventional SWV imaging. Future work will extend this evaluation to in vivo tissues and refine imaging algorithms to reduce refractive artifacts.

Acknowledgement

This work was supported in part by JSPS KAKENHI Grant Number 25K15954, JKA and its promotion funds from KEIRIN RACE.

References

[1] H. L. Oestreicher. "Field and impedance of an oscillating sphere in a viscoelastic medium with an application of biophysics". In: *J. Acoust. Soc. Am.* 23 (1951), pp. 707–714.

[2] L. Sandrin et al. "Transient elastography: A new noninvasive method for assessment of hepatic fibrosis". In: *Ultrasound Med. Biol.* 29 (2003), pp. 1705–1713.

[3] K. Nightingale et al. "Acoustic radiation force impulse imaging: In vivo demonstration of clinical feasibility". In: *Ultrasound Med. Biol.* 28 (2002), pp. 227–235. DOI: 10.1016/s0301-5629(01)00499-9.

[4] J. Bercoff, M. Tanter, and M. Fink. "Supersonic shear imaging: A new technique for soft tissue elasticity mapping". In: *IEEE Trans. Ultrason. Ferroelectr. Freq. Control* 51 (2004), pp. 396–409. DOI: 10.1109/TUFFC.2004.1295425.

[5] Y. Yamakoshi et al. "Shear Wave Imaging of Breast Tissue by Color Doppler Shear Wave Elastography". In: *IEEE Transactions on Ultrasonics, Ferroelectrics, and Frequency Control* 64 (2017), pp. 340–348. DOI: 10.1109/TUFFC.2016.2626359.

[6] R. Koda et al. "Application of continuous shear wave elastography method with multiple frequency selection to liver viscoelasticity measurement". In: *Japanese Journal of Applied Physics* 63 (2024), 04SP82. DOI: 10.35848/1347-4065/ad3ae4.

[7] M. Tabaru et al. "Examination of rapid adjustment system based on screen score obtained using continuous shear wave elastographyt". In: *Journal of Medical Ultrasonics* 51 (2024), pp. 407–418. DOI: 10.1007/s10396-024-01439-7.

[8] N. Tano et al. "Continuous Shear Wave Elastography for Liver Using Frame-to-Frame Equalization of Complex Amplitude". In: *Ultrasonic Imaging* 46 (2024), pp. 197–206. DOI: 10.1177/01617346241247127.

[9] A.Evans et al. "Quantitative shear wave ultrasound elastography: initial experience in solid breast masses". In: *Breast Cancer Res.* 12 (2010), R104.

[10] W. Berg et al. "Shear-wave Elastography Improves the Specificity of Breast US: The BE1 Multinational Study of 939 Masses". In: *Radiology* 262 (2012), pp. 435–449.